Bioorganic & Medicinal Chemistry Letters 24 (2014) 3936–3943

Contents lists available at ScienceDirect

Bioorganic & Medicinal Chemistry Letters

journal homepage: www.elsevier.com/locate/bmcl

Discovery of 9-(1-phenoxyethyl)-2-morpholino-4-oxo-pyrido [1,2-*a*]pyrimidine-7-carboxamides as oral PI3Kβ inhibitors, useful as antiplatelet agents

Fabrizio Giordanetto [a,*,†], Bernard Barlaam [b], Susanne Berglund [a], Karl Edman [c], Olle Karlsson [a], Jan Lindberg [a], Sven Nylander [d], Tord Inghardt [a,*]

[a] Medicinal Chemistry, AstraZeneca R&D, CVMD iMed, Mölndal, Pepparedsleden 1, SE-431 83 Mölndal, Sweden
[b] Medicinal Chemistry, AstraZeneca R&D, Oncology iMed, Alderley Park, Macclesfield, Cheshire SK10 4TG, United Kingdom
[c] Discovery Sciences, AstraZeneca R&D, Pepparedsleden 1, SE-431 83 Mölndal, Sweden
[d] Bioscience, AstraZeneca R&D, CVMD iMed, Pepparedsleden 1, SE-431 83 Mölndal, Sweden

ARTICLE INFO

Article history:
Available online 9 July 2014

Keywords:
Phosphoinositide 3-kinase
p110β
PI3Kβ
Inhibitor
Thromboembolism
Anti-thrombotic agent
Antiplatelet
Insulin resistance

ABSTRACT

Optimization of AZD6482 (**2**), the first antiplatelet PI3Kβ inhibitor evaluated in man, focused on improving the pharmacokinetic profile to a level compatible with once daily oral dosing as well as achieving adequate selectivity towards PI3Kα to minimize the risk for insulin resistance. Structure-based design and optimization of DMPK properties resulted in (*R*)-**16**, a novel, orally bioavailable PI3Kβ inhibitor with potent in vivo anti-thrombotic effect with excellent separation to bleeding risk and insulin resistance.

Phosphoinositide 3-kinases (PI3K) are lipid kinases that regulate signal transduction pathways critical for cell regulation and function. Three different classes of PI3K's (Class I, II and III) have been reported to date. Class I PI3K's phosphorylate the 3′-hydroxy position of the inositol ring of phosphatidylinositol-4,5-biphosphate (PIP_2) to the corresponding phosphatidylinositol-3,4,5-triphosphate (PIP_3).[1] Class I PI3K's have been further classified into Class IA, comprising the p110α, β and δ catalytic subunits, and Class IB (p110γ catalytic subunit). PI3Kα was demonstrated to be involved in cell proliferation and cancer by genetic analysis,[2–6] while also playing a key role in regulating insulin-mediated signaling and glucose metabolism.[7,8]

PI3Kβ has been implicated in the development of phosphatase and TENsin homolog-(PTEN) deficient tumours[9,10] and several chemical classes of PI3Kβ inhibitors have recently been reported by different groups as having anti-proliferative properties[11–18].

Additionally, PI3Kβ is a key regulator of platelet activation via multiple pathways, including $P2Y_{12}$,[19] glycoprotein VI[20,21] and integrin αIIbβ3 outside-in signaling.[22,23] Importantly, treatment with the selective p110β inhibitor TGX-221 (**1**, Fig. 1) resulted in a significant reduction of arterial thrombosis.[24] This is especially noteworthy as no increase in bleeding time was observed with TGX-221, in contrast to aspirin and clopidogrel.[24]

AZD6482 (**2**, Fig. 1) is an ATP-competitive PI3Kβ inhibitor originally discovered by Shaun Jackson and colleagues as a racemic mixture named KN-309.[20] We recently reported the first human target validation of PI3Kβ inhibition with AZD6482.[25] Following a 3 h infusion of seven different doses of AZD6482, a wide separation between anti-thrombotic effect and bleeding was observed, demonstrating that previous pharmacodynamic findings in dog translated well to man.[25]

Whereas AZD6482 (**2**) was well tolerated in man, a weak but significant concentration-dependent increase in plasma insulin and corresponding homeostasis model analysis (HOMA) index was recorded. In the plasma concentration range tested (C_{ss} up to 5.7 μM), such an effect could be ascribed to the compound's ability to inhibit PI3Kα (IC_{50} = 0.87 μM) although other mechanisms cannot be ruled out.[7,8,25] AZD6482 had a short plasma half-life (5–43 min) due to high metabolic clearance and a relatively small

* Corresponding authors. Tel.: +49 (0)231 9742 7224; fax: +49 (0)231 9742 7219 (F.G.); tel.: +46 31 7761954; fax: +46 31 7763724 (T.I.).
E-mail addresses: fgiordanetto@tarosdiscovery.com (F. Giordanetto), tord.inghardt@astrazeneca.com (T. Inghardt).
† Present address: Taros Chemicals GmbH & Co. KG, Emil-Figge-Str. 76a, 44227 Dortmund, Germany.

http://dx.doi.org/10.1016/j.bmcl.2014.07.007
0960-894X/

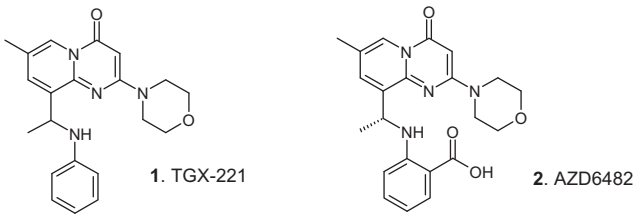

Figure 1. Selected PI3Kβ inhibitors as chemical starting points.

distribution volume (40–68 L) [25]. Thus, the pharmacokinetic and pharmacodynamic profile of AZD6482 limits its use to parenteral administration in situations where a low bleeding risk is desirable, such as during acute stroke, during percutaneous coronary intervention or as bridging therapy when oral antiplatelet treatment needs to be interrupted for surgery. Furthermore, while the effect of AZD6482 on insulin homeostasis would not be clinically relevant during short-term infusion, it could potentially cause insulin resistance during chronic administration.

Based on these premises, a number of programs with the aim of developing oral PI3Kβ inhibitors for the treatment of various diseases were initiated in our laboratories. With a view to address arterial thrombosis, these included a fragment-based approach, as previously reported,[26] as well as a follow-up optimization of AZD6482, as discussed in the present study. This latter work also informed medicinal chemistry efforts to discover PI3Kβ inhibitors for the treatment of PTEN-deficient tumours, as detailed in the accompanying Letter.[27]

Starting from AZD6482, the overall strategy consisted of two main objectives: (a) to improve the pharmacokinetic profile to a level that would enable once daily oral dosing in an eventual chronic therapy setting and (b) to improve selectivity over the PI3Kα isoform as a way to minimize the risk of interference with insulin signaling. As an aid to the generation of structure activity relationship (SAR) hypotheses, the crystal structure of PI3Kγ in complex with **2** was solved at a final resolution of 2.9 Å.[28] Analogously to the crystal structure of PI3Kγ in complex with LY294002,[29] the morpholino ring oxygen atom of **2** is within hydrogen bonding distance of the amide nitrogen of V882 in the hinge region of PI3Kγ as shown in Figure 2. All residues highlighted in the discussion are identical in the PI3Kβ isoform except for K890 which is replaced by D856 in PI3Kβ. Previous studies have demonstrated that the interactions to the backbone of the hinge region are critical for PI3K activity.[7,29] The pyrimidinone core is tightly packed against the side chain of Y867 and I879 in the so-called 'affinity pocket' of PI3Kγ, a key potency determinant for PI3K inhibitors. The anthranilic side chain of **2** induces the so-called PI3Kγ 'specificity' pocket that is absent in the apo enzyme.[29] mainly by shifting the side chain of M804. The ability of compounds to induce this conformational switch was shown to be related to their degree of selectivity across different isoforms.[7,30] According to the present PI3Kγ structure, the carboxylic acid of **2** is not involved in any specific interaction with the enzyme, although the side chains of K802 and K890 are relatively proximal (<3.6 Å). Lastly, the methyl group at position 7 of the pyridopyrimidinone core is lined up with the side chains of K833 and D964, as shown in Figure 2. Interestingly, these two amino acids are conserved in PI3Kβ, and position 7 of the scaffold could represent a suitable substitution vector towards the PI3K channel normally occupied by the triphosphate group of ATP.[29]

Based on the PI3Kγ-**2** complex, we focused on two main areas for modification: (a) the anthranilic acid side chain and (b) the methyl group at position 7 of the pyridopyrimidinone core. Considering the short half-life of **2** in humans, metabolic clearance represented a key optimization parameter. When incubated with human hepatocytes, **2** was rapidly metabolized (Cl_{int} = 17.5 μL/min/10^6 cells, Table 1) by UDP-glucuronosyl transferases to the corresponding acyl glucuronide at its anthranilic acid side chain. An initial attempt to modify the acidic functionality was thus made in order to verify the effects on metabolic turnover, as well as to evaluate the resulting PI3Kβ SAR. Accordingly, compounds **3**–**8** were synthesized based on Scheme 1. Starting from alcohol **25** [31] compounds **3**, **4**, **6** and **8** were made through bromination and subsequent displacement with the corresponding aniline in one pot. Compounds **5** and **7** were made from **2** through coupling with hydroxylamine and methylsulfonamide, respectively.

Replacement of the anthranilic acid group of **2** with a 3-aminobenzoic acid regioisomer (**3**) drastically improved metabolic stability, although this was counterbalanced by a significant potency loss against PI3Kβ, as shown in Table 1. Likewise, the sulfonic acid analog **6** was very stable in human hepatocytes, although its minimal cellular permeability (P_{app} <0.05) might confound such result. Alteration of the pK_a of the acid by installment of an electron withdrawing chlorine atom (**4**), as well as typical carboxylic acid bioisosters **5**, **7** and **8** did not offer any advantage in terms of intrinsic clearance, despite maintaining favorable PI3Kβ potencies

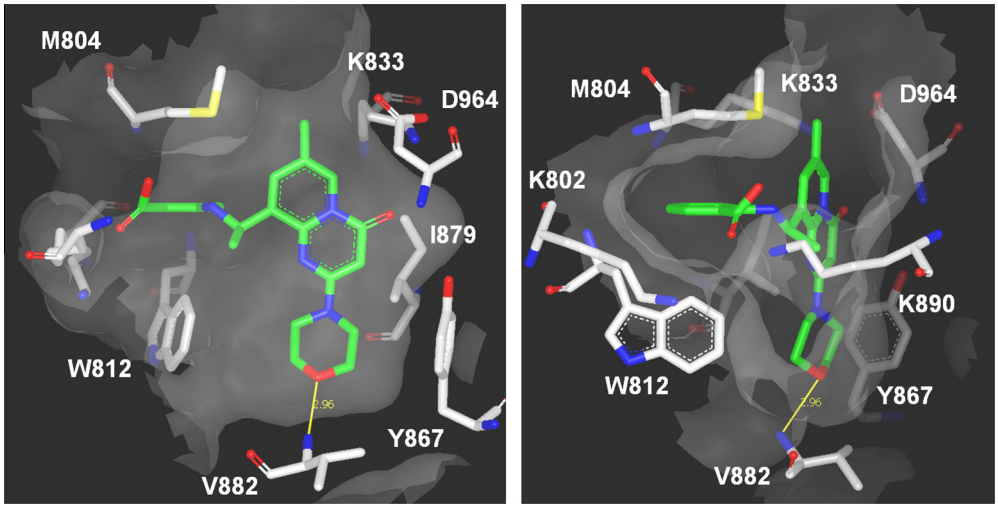

Figure 2. Crystal structure of **2** (capped sticks, green carbon atoms) bound to PI3Kγ (capped sticks, white carbon atoms). Selected side chains (residue identity and numbering according to PI3Kγ amino acid sequence) are displayed. Putative hydrogen bonds are shown as solid yellow lines.

Table 1
Modification and bioisosteric replacement of carboxylic acid in AZD6482 (**2**)

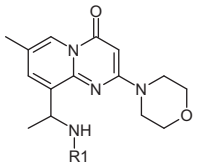

Compound[a]	R^1	PI3Kβ IC_{50}[b] (μM)	PI3Kα IC_{50}[b] (μM)	P_{app}[c] (10^{-6} cm/s)	hHEP CL_{int}[d] (μL/min/10^6 cells)	Log $D_{7.4}$[e]
1		0.049	5.8	66	20	3.6
2	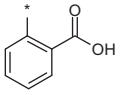	0.010	0.87	18	17.5	0.75
3	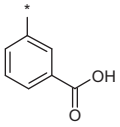	4.8	12.1	0.9	<4	0.3
4	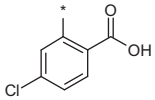	0.031	1.46	15	11.9	1.2
5	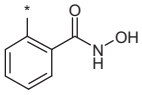	0.084	2.88	52	30.2	1.5
6	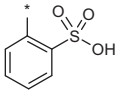	0.030	0.33	0.05	<4	0.3
7	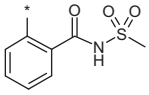	0.012	0.16	0.11	15	0.9
8	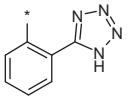	0.051	1.41	0.08	18.1	0.8

[a] All compounds except **2**, **5** and **7** are racemic.
[b] Results are mean of at least two experiments. Experimental errors within 20% of value.[32]
[c] Permeability measured in Caco-2 cells in the A to B direction, pH 6.5.[28]
[d] Intrinsic clearance of test compounds after incubation with human hepatocytes.[28]
[e] Experimental Log *D* at pH 7.4 using HPLC.[33]

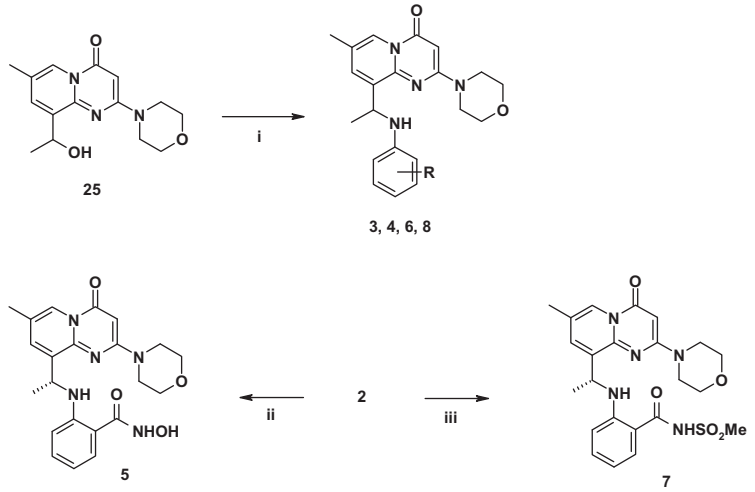

Scheme 1. Synthesis of compounds **3**–**8**. Reagents and conditions: (i) PBr_3 (1 equiv), CH_2Cl_2, reflux, 7 h, then $ArNH_2$ (2.4 equiv), NEt_3 (4.5 equiv), reflux, 20 h (27–66%) (ii) H_2N–OH·HCl, EtOCOCl, NEt_3, 2 h (15%) (iii) H_2NSO_2Me, EDC, DMAP, 3 d (99%).

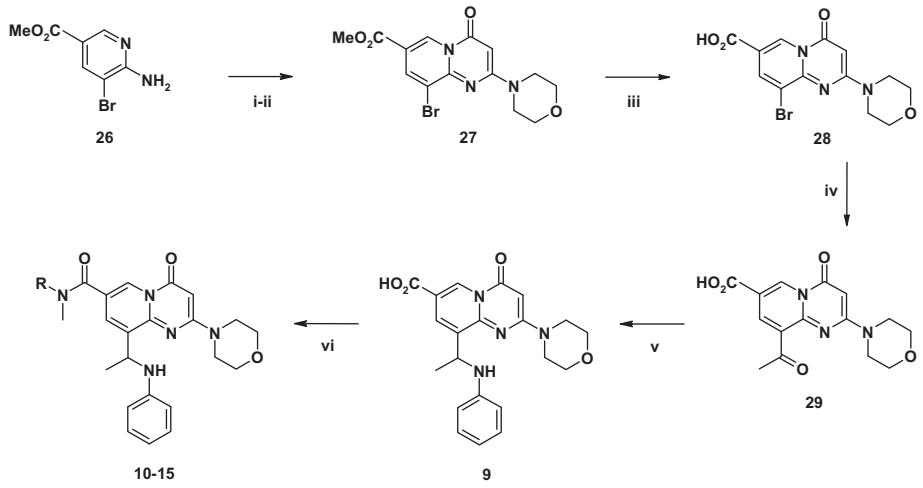

Scheme 2. Synthesis of compounds **9**–**15**. Reagents and conditions: (i) malonic acid bis(2,4,6-trichlorophenyl) ester (1.2 equiv), toluene, 90 °C (93%); (ii) MsCl (1.1 equiv), NEt_3 (1.2 equiv), THF, 10–20 °C then morpholine (3 equiv), THF, 50 °C, (82%); (iii) NaOH (1.5 equiv), water, 70 °C, 1 h, (92%); (iv) 4-(vinyloxy)butan-1-ol (5 equiv), 1,3-bis(diphenylphosphino)propane (0.1 equiv), $Pd(OAc)_2$ (0.025 equiv), K_2CO_3 (2.5 equiv), DMF–water (9:1), 80 °C, then **28**, 135 °C, 3 h, then HCl(aq.) (quant); (v) $PhNH_2$ (5 equiv), AcOH, polystyrene supported trimethylammonium cyanoborohydride, DMF–water (3:1), rt, 18 h, (48%); (vi) RNHMe (2 equiv), NEt^iPr_2 (5 equiv), HATU (1.5 equiv), CH_2Cl_2, rt.

(IC_{50} = 0.012–0.084 μM), as summarized in Table 1. Preliminary chemical variation of the acid group of **2** did not indicate any obvious avenue for further exploration.

Additionally, direct comparison with **1**, indicated that the acid group could be removed without a substantial deterioration in potency, selectivity and metabolic stability (Table 1).

The relatively high lipophilicity of **1** ($Log D_{7.4}$ = 3.6) could be partly held responsible for the high turnover in hepatocytes (Cl_{int} = 20 μL/min/10^6 cells, Table 1) and could represent a general threat to further development.[34] Based on this hypothesis, we set out to introduce polar groups at position 7 of the pyridopyrimidinone scaffold. This strategy also offered the opportunity to evaluate additional molecular interaction with PI3Kβ and PI3Kα, as predicted from the structural information available (Fig. 2), and their effects on potency and selectivity. Compounds **9**–**15** were thus synthesized according to Scheme 2. Starting from aminopyridine **26**, the pyridopyrimidone core was obtained through cyclization with bis-trichlorophenyl malonate. Mesylation of the resulting 3-hydroxypyridopyrimidone, followed by displacement with morpholine and hydrolysis of the ester afforded acid **28**. This was subjected to Heck coupling with 4-(vinyloxy)butan-1-ol which afforded methyl ketone **29** after hydrolysis. Reductive amination with aniline gave **9** which after amide couplings gave compounds **10**–**15**.

Oxidation of the methyl group of **1** to the corresponding carboxylic acid derivative **9** was tolerated by PI3Kβ (IC_{50}: 0.059 μM) and significantly improved metabolic stability (Cl_{int}: <4 μL/min/10^6 cells, Table 2). Nevertheless, selectivity towards PI3Kα was reduced by a factor of 10 and, as expected, cellular permeability was limited, as shown in Table 2. Neutralization of the permanent negative charge of **9** (in a physiological pH range of 6.5–7.4) with the corresponding *N*,*N*-dimethylamide analog **10** restored PI3Kβ/PI3Kα selectivity and passive diffusion to adequate levels (Table 2). Among the different tertiary amides evaluated (**11**–**15**) in this series, the *N*-(2-hydroxymethyl)-*N*-methyl-amide derivative **11** offered the best compromise of potency, selectivity, permeability and stability, especially when considering its moderate lipophilicity (cf. **10** and **11**, **11** and **12**, Table 2).

While **11** afforded the right balance of in vitro properties for further characterization, concerns existed over the presence of an unsubstituted aniline moiety in its structure. This had the potential to form reactive metabolites after oxidative metabolism and would require additional assessment of its genotoxicity potential. The perceived toxicological risks associated with the development of aniline-based compounds, especially when considering the high demands for patient safety in cardiovascular indications, prompted us to evaluate structural alternatives. The nitrogen-to-oxygen isosteric replacement was thought to preserve most of the conformational and physicochemical properties of **11**, whilst removing the aniline group. A set of phenol-containing derivatives was thus synthesized according to Scheme 3. Selective Luche reduction of the methyl ketone **29** followed by amide coupling with TBDMS-protected 2-(methylamino)ethanol gave alcohol **31**. Mitsunobu reaction with ADDP and the corresponding phenol followed by deprotection of the silylated alcohol gave compounds **16**–**24**.

As shown in Table 3, replacing the anilinic nitrogen atom of **11** with an oxygen (**16**) decreased PI3Kβ potency but increased selectivity towards PI3Kα (38× vs 53×, respectively). At this point in the program, we had observed a lack of linear correlation between the PI3Kβ enzyme assay and functional activity (total or unbound) in the human platelet rich plasma aggregation assay (PRP). Knowing that PRP activity was a good predictor of in vivo efficacy in dog and man,[25] we introduced this assay earlier in the screening cascade and payed more attention to the 'safety margin' between PRP and PI3Kα. As a reference point, compound **2** (AZD6482) has a PRP IC_{50} = 0.28 μM and PI3Kα IC_{50} = 0.87 μM, that is, a ratio of 3.1 whereas compound **16** gave a significantly improved ratio of 25 (Table 3). Further mono- and di-substitution of the phenol side chain (**17**–**24**) had varying effects on potency and selectivity but always afforded weaker platelet inhibition than the unsubstituted compound (Table 1). As an example, the *meta*-methoxy analog **22** displayed the best PI3Kβ potency and selectivity (PI3Kβ IC_{50} = 0.047 μM, PI3Kα/PI3Kβ = 957×) but its mediocre platelet inhibition (IC_{50} = 1.9 μM) and high metabolic instability (data not shown) prevented any further elaboration.

Based on the available results, separation of **16** into its constituent enantiomers was carried out for further profiling.[35] PI3Kβ, PI3Kα and PRP potency resided mainly in the (*R*) enantiomer (e.g. PI3Kβ IC_{50} = 0.1 vs 0.8 μM). As summarized in Table 4, (*R*)-**16** offered a favorable overall pharmacological and pharmacokinetic profile when compared to compound **2**. It potently inhibited platelet activation in plasma and whole blood, was highly soluble, metabolically

Table 2
Modification of position 7 in TGX-221 (**1**)

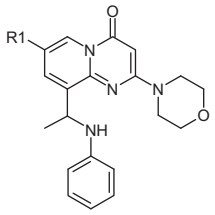

Compound[a]	R^1	PI3Kβ IC_{50}[b] (μM)	PI3Kβ IC_{50}[b] (μM)	P_{app}[c] (10^{-6} cm/s)	hHEP CL_{int}[d] (μL/min/10^6 cells)	Log $D_{7.4}$[e]
1		0.049	5.8	65	19.8	3.6
9		0.059	0.61	0.04	<4	0.6
10		0.068	2.5	35.4	4.3	2.7
11	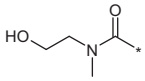	0.058	2.2	4.3	<4	2.0
12	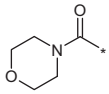	0.14	6.9	26.9	<4	2.7
13	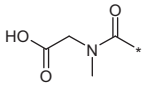	0.34	3.8	1.0	<4	0.6
14	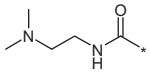	0.035	2.3	0.99	<4	1.7
15	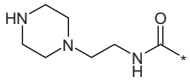	0.076	4.8	0.05	<4	1.5

[a] All compounds are racemic.
[b] Results are mean of at least two experiments. Experimental errors within 20% of value.[32]
[c] Permeability measured in Caco-2 cells in the A to B direction, pH 6.5.[28]
[d] Intrinsic clearance of test compounds after incubation with human hepatocytes.[28]
[e] Experimental Log*D* at pH 7.4 using HPLC.[33]

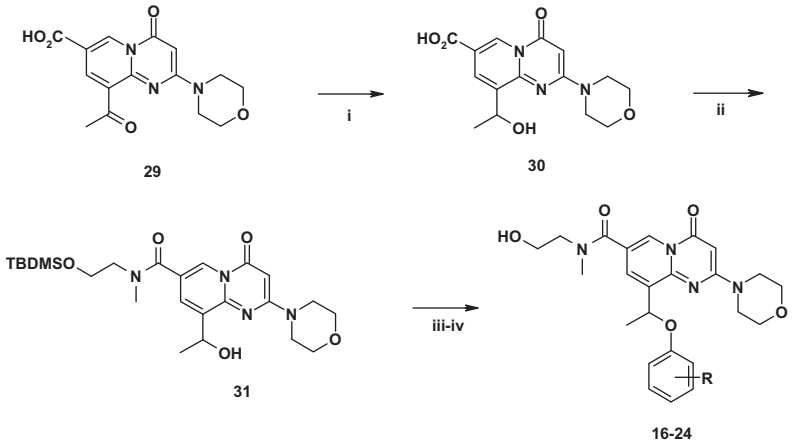

Scheme 3. Synthesis of compounds **16**–**24**. Reagents and conditions: (i) $CeCl_3{\cdot}7H_2O$ (1.05 equiv), MeOH–CH_2Cl_2 (2:1), then $NaBH_4$ (1.3 equiv), 15 °C, 15 min, (84%); (ii) $TBDMSOCH_2CH_2NHMe$, TSTU (1.1 equiv), NEt^iPr_2 (3 equiv), CH_2Cl_2, (59%); (iii) ArOH, ADDP (1.2 equiv), PPh_3 (1.2 equiv), CH_2Cl_2, reflux, 16 h; (iv) TFA, CH_2Cl_2 (29–57% over 2 steps).

stable, cellular permeable and did not generate any detectable reactive metabolites (Table 4). In vivo pharmacokinetics in different species (exemplified by the pharmacologically relevant dog species in Table 4) reflected well the observed in vitro profile. (*R*)-**16** was indeed orally bioavailable ($F = 31\%$) with a limited volume of distribution (1.1 L/kg) and moderate clearance (8 mL/min/kg). Furthermore, no significant inhibition of Cyp450 enzymes and ion channels involved in cardiac function[39] was recorded at the highest

Table 3
Phenol analogs of **11**

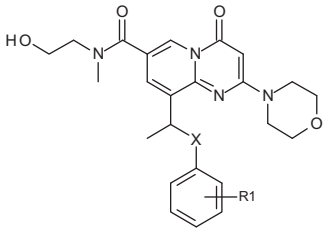

Compound[a]	R^1	X	PI3Kβ IC_{50}[b] (μM)	PI3Kα IC_{50}[b] (μM)	PRP IC_{50}[c] (μM)	Log $D_{7.4}$[d]
11	H	NH	0.058	2.2	0.14	2.0
16	H	O	0.19	10.1	0.4	2.3
17	*o*-Me	O	0.11	1.3	0.7	3
18	*m*-Me	O	0.18	9.4	5	2.8
19	*o*-F	O	0.66	3.4	2.1	2.3
20	*m*-CN	O	1.7	8.2	1.5	2
21	*o*-OMe	O	0.4	2.5	9.6	1.9
22	*m*-OMe	O	0.047	4.5	1.9	2.3
23	*m*-Me, *p*-F	O	0.2	2.4	2.5	2.9
24	*o*-Me, *m*-F	O	0.046	0.6	0.7	3.3

[a] All compounds are racemic.
[b] Results are mean of at least two experiments. Experimental errors within 20% of value.[32]
[c] Human collagen-induced platelet rich plasma (PRP) aggregation.[36]
[d] Experimental Log*D* at pH 7.4 using HPLC.[33]

Table 4
In vitro/vivo profile of (*R*)-**16** compared to **2** (AZD6482)

	(*R*)-**16**	**2**
PI3Kβ/α/γ/δ IC_{50}[a] (μM)	0.1/3.5/83/0.4	0.01/0.87/1.09/0.08
Hu collagen-induced PRP aggregation IC_{50}[b] (nM)	210	280
Hu ADP-induced whole blood platelet aggregation IC_{50}[c] (μM)	1.2	0.27
Dog ADP-induced whole blood platelet aggregation IC_{50}[c] (μM)	0.95	1.4
Solubility[d] (μM)	>1796	100
hHEP $T_{1/2}$[e] (min)	>173	40
P_{app}[f] (10^{-6} cm/s)	11.1	18
RM[g]	No (0.0)	No (0.0)
Human/dog PPB F_u[h] (%)	26/42	8/10
Dog dose iv/po[i] (μmol/kg)	1/2	0.5/nd
Dog CL[i] (mL/min/kg)	8	17
Dog V_{ss} (L/kg)	1.2	14
Dog F^i (%)	31	nd

[a] Results are mean of at least two experiments. Experimental errors within 20% of value.[32]
[b] $N = 6$. SD = 0.03.[36]
[c] $N > 3$, SD <0.2.[37]
[d] DMSO/HBSS solubility measured at pH 7.4.[33]
[e] Intrinsic clearance of test compounds after incubation with human hepatocytes.[28]
[f] Permeability measured in Caco-2 cells in the A to B direction, pH 6.5.[28]
[g] Ratio of reactive metabolite (RM) formation measured from 30′ incubation with human liver microsomes (1 mg/mL) in the presence of glutathione.[38]
[h] % fraction unbound in plasma measured by equilibrium dialysis (18 h at 37 °C).
[i] Pharmacokinetic parameters calculated from noncompartmental analysis concentrations in fasted Beagle male dogs (iv/po $N = 5{:}4$).

tested concentrations (20 and 33 μM, respectively). A large screening panel including 55 different protein kinases did not reveal any significant inhibition when tested at 1 μM compound concentration. No significant binding was observed against more than 100 different enzyme, receptors and ion channels at 30 μM compound concentration.

(*R*)-**16** achieved the two original optimization parameters:—it afforded a pharmacokinetic profile compatible with once daily oral dosing and an improved safety margin towards PI3Kα. It was thus characterized in vivo to evaluate its anti-thrombotic potential and any potential risks associated with bleeding and insulin resistance. A modified Folts' model[25,40] was used to evaluate efficacy versus bleeding and anaesthetized dogs received vehicle (saline) followed by consecutive doses of (*R*)-**16** intravenously over 30 min periods (bolus 0.03–1.3 μg/kg and infusion 0.005–0.24 μg/kg/min). The main parameters measured were blood flow (cyclic flow reductions, CFRs), bleeding time, blood loss, ex vivo platelet aggregation (Multiplate) and drug exposure. As shown in Figure 3, (*R*)-**16** elicited a concentration-dependent inhibition of platelet aggregation ex vivo (EC_{80} = 0.69 ± 0.06 μM), which well predicted its inhibition of thrombosis in vivo (EC_{80}: 0.6 ± 0.05 μM). Importantly, no significant increase in bleeding time and blood loss (here defined as a fold increase greater than 3.5, a cut off used previously in this model for $P2Y_{12}$ antagonists[41]) was recorded at the observed maximum compound concentrations (24.1 ± 2.3 μM). In order to investigate if the improved margin between PRP and PI3Kα translated into less impact on insulin signaling relative to AZD6482, (*R*)-**16** was evaluated in terms of relative homeostasis model analysis (HOMA) insulin resistance index (the product of plasma glucose and plasma insulin) in SD rats, as summarized in Figure 4. Gratifyingly, no significant increase of the HOMA-index from baseline was apparent at the maximum compound concentration sampled

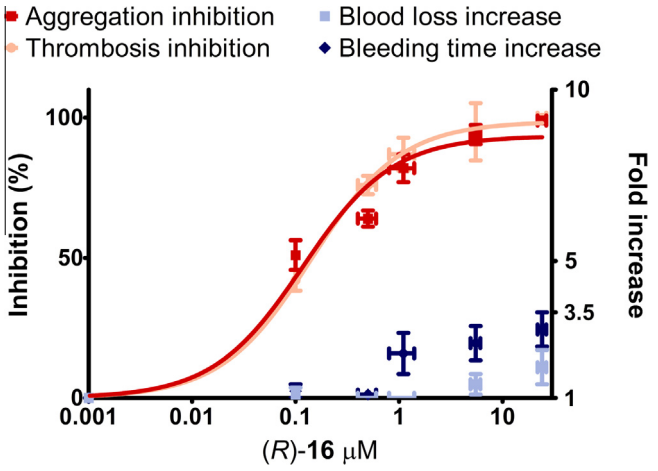

Figure 3. PKPD relationship between the plasma concentration of (*R*)-**16** (μM), ex vivo inhibition of whole blood ADP-induced platelet aggregation (red squares and fit line), in vivo inhibition of thrombus formation (pink circles and fit line), fold increase in blood loss (light blue squares) and bleeding time (dark blue squares), following administration to Beagle dogs. Data represents means ± SEM ($N = 4$).[25,41]

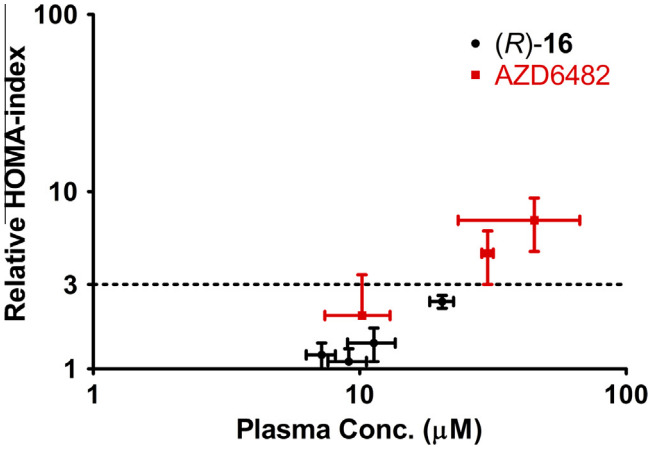

Figure 4. PKPD relationship between compound plasma concentrations (μM) and the relative homeostasis model analysis (HOMA) insulin resistance index (the product of plasma glucose and plasma insulin) in SD rats. Data represents means ± SEM ($N \geqslant 5$).[25] AZD6482 (**2**) is depicted as red squares, (*R*)-**16** as black squares. A relative HOMA index of 3 (dashed line) represents a statistically significant change from baseline.

(20.4 ± 2.1 μM). A significant effect on insulin resistance at higher compound concentrations cannot be excluded. Nevertheless, the safety margin to compound concentrations resulting in full anti-thrombotic effect appears to be acceptable for (*R*)-**16**.

In summary, optimization of AZD6482, aimed at improving its PK profile and increase the margin to PI3Kα inhibition, resulted in the design, synthesis and characterization of (*R*)-**16**, a novel PI3Kβ inhibitor well suited for oral administration. Based on its potent in vivo anti-thrombotic effect and minimized risk of bleeding and insulin resistance, (*R*)-**16** was selected as a preclinical candidate for further development.

Acknowledgements

We thank the following AstraZeneca R&D colleagues: Jan-Arne Björkman and Helen Zachrisson for Folts dog experiments; Elham Nikookhesal and Göran Wahlund for rat HOMA index experiments; Anna-Karin Asztély and Jan-Christer Ulvinge for in vitro platelet function experiments; Anders Tunek for DMPK input; Bryan Egner and Joakim Gradén for synthesis contributions.

Supplementary data

Supplementary data associated with this article can be found, in the online version, at http://dx.doi.org/10.1016/j.bmcl.2014.07.007.

References and notes

1. Vanhaesebroeck, B.; Waterfield, M. D. *Exp. Cell Res.* **1999**, *253*, 239.
2. Samuels, Y.; Wang, Z.; Bardelli, A.; Silliman, N.; Ptak, J.; Szabo, S.; Yan, H.; Gazdar, A.; Powell, S. M.; Riggins, G. J.; Willson, J. K.; Markowitz, S.; Kinzler, K. W.; Vogelstein, B.; Velculescu, V. E. *Science* **2004**, *304*, 554.
3. Levine, D. A.; Bogomolniy, F.; Yee, C. J.; Lash, A.; Barakat, R. R.; Borgen, P. I.; Boyd, J. *Clin. Cancer Res.* **2005**, *11*, 2875.
4. Whyte, D. B.; Holbeck, S. L. *Biochem. Biophys. Res. Commun.* **2006**, *340*, 469.
5. Shayesteh, L.; Lu, Y.; Kuo, W. L.; Baldocchi, R.; Godfrey, T.; Collins, C.; Pinkel, D.; Powell, B.; Mills, G. B.; Gray, J. W. *Nat. Genet.* **1999**, *21*, 99.
6. Campbell, I. G.; Russell, S. E.; Choong, D. Y.; Montgomery, K. G.; Ciavarella, M. L.; Hooi, C. S.; Cristiano, B. E.; Pearson, R. B.; Phillips, W. A. *Cancer Res.* **2004**, *64*, 7678.
7. Knight, Z. A.; Gonzalez, B.; Feldman, M. E.; Zunder, E. R.; Goldenberg, D. D.; Williams, O.; Loewith, R.; Stokoe, D.; Balla, A.; Toth, B.; Balla, T.; Weiss, W. A.; Williams, R. L.; Shokat, K. M. *Cell* **2006**, *125*, 733.
8. Chaussade, C.; Rewcastle, G. W.; Kendall, J. D.; Denny, W. A.; Cho, K.; Grønning, L. M.; Chong, M. L.; Anagnostou, S. H.; Jackson, S. P.; Daniele, N.; Shepherd, P. R. *Biochem. J.* **2007**, *404*, 449.
9. Jia, S.; Liu, Z.; Zhang, S.; Liu, P.; Zhang, L.; Hyun, S.; Zhang, L. J.; Signoretti, S.; Loda, M.; Roberts, T. M.; Zhao, J. J. *Nature* **2008**, *45*, 776.
10. Wee, S.; Wiederschain, D.; Maira, S. M.; Loo, A.; Miller, C.; deBeaumont, R.; Stegmeier, F.; Yao, Y. M.; Lengauer, C. *Proc. Natl. Acad. Sci. U.S.A.* **2008**, *105*, 13057.
11. Certal, V.; Halley, F.; Virone-Oddos, A.; Filoche-Romme, B.; Carry, J.-C.; Gruss-Leleu, F.; Bertin, L.; Guizani, H.; Pilorge, F.; Richepin, P., et al. *Bioorg. Med. Chem. Lett.* **2014**, *24*, 1506.
12. Certal, V.; Carry, J.-C.; Halley, F.; Virone-Oddos, A.; Thompson, F.; Filoche-Romme, B.; El-Ahmad, Y.; Karlsson, A.; Charrier, V.; Delorme, C., et al. *J. Med. Chem.* **2014**, *57*, 903.
13. Yu, H.; Moore, M. L.; Erhard, K.; Hardwicke, M. A.; Lin, H.; Luengo, J. I.; McSurdy-Freed, J.; Plant, R.; Qu, J.; Raha, K., et al. *ACS Med. Chem. Lett.* **2013**, *4*, 230.
14. Certal, V.; Halley, F.; Virone-Oddos, A.; Delorme, C.; Karlsson, A.; Rak, A.; Thompson, F.; Filoche-Rommé, B.; El-Ahmad, Y.; Carry, J. C.; Abecassis, P. Y.; Lejeune, P.; Vincent, L.; Bonnevaux, H.; Nicolas, J. P.; Bertrand, T.; Marquette, J. P.; Michot, N.; Benard, T.; Below, P.; Vade, I.; Chatreaux, F.; Lebourg, G.; Pilorge, F.; Angouillant-Boniface, O.; Louboutin, A.; Lengauer, C.; Schio, L. *J. Med. Chem.* **2012**, *55*, 4788.
15. Sanchez, R. M.; Erhard, K.; Hardwicke, M. A.; Lin, H.; McSurdy-Freed, J.; Plant, R.; Raha, K.; Rominger, C. M.; Schaber, M. D.; Spengler, M. D.; Moore, M. L.; Yu, H.; Luengo, J. I.; Tedesco, R.; Rivero, R. A. *Bioorg. Med. Chem. Lett.* **2012**, *22*, 3198.
16. Lin, H.; Erhard, K.; Hardwicke, M. A.; Luengo, J. I.; Mack, J. F.; McSurdy-Freed, J.; Plant, R.; Raha, K.; Rominger, C. M.; Sanchez, R. M.; Schaber, M. D.; Schulz, M. J.; Spengler, M. D.; Tedesco, R.; Xie, R.; Zeng, J. J.; Rivero, R. A. *Bioorg. Med. Chem. Lett.* **2012**, *22*, 2230.
17. Lin, H.; Schulz, M. J.; Xie, R.; Zeng, J.; Luengo, J. I.; Squire, M. D.; Tedesco, R.; Qu, J.; Erhard, K.; Mack, J. F.; Raha, K.; Plant, R.; Rominger, C. M.; Ariazi, J. L.; Sherk, C. S.; Schaber, M. D.; McSurdy-Freed, J.; Spengler, M. D.; Davis, C. B.; Hardwicke, M. A.; Rivero, R. A. *ACS Med. Chem. Lett.* **2012**, *3*, 524.
18. Kim, J.; Hong, S.; Hong, S. *Bioorg. Med. Chem. Lett.* **2011**, *21*, 6977.
19. Garcia, A.; Kim, S.; Bhavaraju, K.; Schoenwaelder, S.; Kunapuli, S. *Biochem J.* **2010**, *429*, 369.
20. Kim, S.; Mangin, P.; Dangelmaier, C.; Lillian, R.; Jackson, S. P.; Daniel, J. L.; Kunapuli, S. P. *J. Biol. Chem.* **2009**, *284*, 33763.
21. Gilio, K.; Munnix, I. C.; Mangin, P.; Cosemans, J. M.; Feijge, M. A.; van der Meijden, P. E.; Olieslagers, S.; Chrzanowska-Wodnicka, M. B.; Lillian, R.; Schoenwaelder, S.; Koyasu, S.; Sage, S. O.; Jackson, S. P.; Heemskerk, J. W. *J. Biol. Chem.* **2009**, *284*, 33750.
22. Schoenwaelder, S. M.; Ono, A.; Sturgeon, S.; Chan, S. M.; Mangin, P.; Maxwell, M. J.; Turnbull, S.; Mulchandani, M.; Anderson, K.; Kauffenstein, G.; Rewcastle, G. W.; Kendall, J.; Gachet, C.; Salem, H. H.; Jackson, S. P. *J. Biol. Chem.* **2007**, *282*, 28648.
23. Canobbio, I.; Stefanini, L.; Cipolla, L.; Ciraolo, E.; Gruppi, C.; Balduini, C.; Hirsch, E.; Torti, M. *Blood* **2009**, *114*, 2193.
24. Jackson, S. P.; Schoenwaelder, S. M.; Goncalves, I.; Nesbitt, W. S.; Yap, C. L.; Wright, C. E.; Kenche, V.; Anderson, K. E.; Dopheide, S. M.; Yuan, Y.; Sturgeon, S. A.; Prabaharan, H.; Thompson, P. E.; Smith, G. E.; Shepherd, P. R.; Daniele, N.; Kulkarni, S.; Abbott, B.; Saylik, D.; Jones, C.; Lu, L.; Giuliano, S.; Hughan, S. C.; Angus, J. A.; Robertson, A. D.; Salem, H. H. *Nat. Med.* **2005**, *11*, 507.
25. Nylander, S.; Kull, B.; Björkman, J. A.; Ulvinge, J.-C.; Oakes, N.; Emanuelsson, B. M.; Andersson, M.; Skärby, T.; Inghardt, T.; Fjellström, O.; Gustafsson, D. *J. Thromb. Haemost.* **2012**, *10*, 2127.
26. (a) Giordanetto, F.; Kull, B.; Dellsén, A. *Bioorg. Med. Chem. Lett.* **2011**, *21*, 829; (b) Giordanetto, F.; Wållberg, A.; Cassel, J.; Ghosal, S.; Kossenjans, M.; Yuan, Z.-Q.; Wang, X.; Lub, F.; Zhoub, X.; Dianqing, L.; Liang, L. *Bioorg. Med. Chem. Lett.* **2012**, *22*, 6665; (c) Giordanetto, F.; Wållberg, A.; Ghosal, S.; Iliefski, T.; Cassel, J.; Yuan, Z. Q.; von Wachenfeldt, H.; Andersen, S. M.; Inghardt, T.; Tunek, A.; Nylander, S. *Bioorg. Med. Chem. Lett.* **2012**, *22*, 6671.

27. Barlaam, B. et al *Bioorg. Med. Chem. Lett.* **2014**, *24*, 3928.
28. For experimental details, see Supporting information.
29. Walker, E. H.; Pacold, M. E.; Perisic, O.; Stephens, L.; Hawkins, P. T.; Wymann, M. P.; Williams, R. L. *Mol. Cell.* **2000**, *6*, 909.
30. Berndt, A.; Miller, S.; Williams, O.; Le, D. D.; Houseman, B. T.; Pacold, J. I.; Gorrec, F.; Hon, W. C.; Liu, Y.; Rommel, C.; Gaillard, P.; Ruckle, T.; Schwarz, M. K.; Shokat, K. M.; Shaw, J. P.; Williams, R. L. *Nat. Chem. Biol.* **2010**, *6*, 117.
31. Fjellström, O; Gustafsson, D.; Jackson, S; Lindberg, J. PCT Int. Appl. WO2009093972 (2009).
32. PI3Kαβγδ enzyme isoform selectivity was evaluated in vitro using human recombinant enzyme and an AlphaScreen assay to measure PIP3 production, as described in Bailey, J. P.; Giles, M. B.; Pass, M. PCT Int. Appl. WO2006005914, (2006).
33. Wan, H.; Holmén, A. G. *Comb. Chem. High Throughput Screening* **2009**, *12*, 315.
34. Waring, M. J. *Expert Opin. Drug Discovery* **2010**, *5*, 235.
35. The (*R*) configuration was assigned to the more potent enantiomer, in analogy with the crystal structure of **2** bound in PI3Kγ. (*R*)-**16** was obtained through chiral preparative HPLC of racemic **16** on a Chiralpak AD column, 50 × 250 mm, particle size 20 μm, using EtOH/Et_3N 100:0.1 as eluent, flow rate 120 mL/min at 40 °C. Detection PDA 280 nm. $[\alpha]_D^{20}$ −174.8° (*c* = 1, CH_3CN), ^1H NMR (400 MHz, DMSO-d_6) δ 1.62 (d, 3H), 2.89 (br s, 3H), 3.1–3.25 (m, 1H), 3.34–3.70 (m, 11H), 4.68–4.83 (m, 1H), 5.68 (s, 1H), 5.95 (q, 1H), 6.87 (m, 3H), 7.21 (m, 2H), 7.74 (br s, 1H), 8.79 (d, 1H). (ESI) *m*/*z* calcd for $C_{24}H_{28}N_4O_5$ $[M+H]^+$ 453.2138; found 453.2120.
36. Blood was collected by venipuncture from healthy donors into vacutainer tubes containing sodium citrate (final concentration in blood 11 mM). Collagen-induced platelet rich plasma (PRP) light transmission aggregometry (LTA) was evaluated using an in house developed 96 well plate assay. For experimental details, see Ref. 25.
37. Blood was collected by venipuncture from healthy donors or beagle dogs into vacutainer tubes containing sodium citrate (final concentration in blood 11 mM). Whole blood impedance aggregometry was evaluated using the Multiplate (Dynabyte, Munich, Germany) impedance aggregometer. For additional details, see Ref. 25.
38. Ratio obtained by dividing the total integrated peak area of glutathione adducts of the test compound by the integrated peak area of the major glutathione adduct of the control compound clozapine (average value, *N* = 3). RM formation is ranked as follows: ratio >1 = 'high'; ratio between 0.25–1 = 'medium'; ratio <0.25 = 'low'.
39. Patch clamp assay using IONWORKS™ technology in CHO cells expressing the relevant human ion channel (hERG, $Na_v1.5$, $Na_v1.2$, $K_v4.3$, IK_s, $Ca_v3.2$, $Ca_v2.2$). For $Ca_v1.2$: Patch clamp assay using IONWORKS™ technology in CHO cells expressing CACNA1C, CACNB2 and CACNA2D1 (ChanTest, Cleveland, OH), as in Dilbaghi, S.; Abi-Gerges, N.; Morton, M. J.; Bridgland-Taylor, M. H.; Pollard, C. E.; Valentin, J.-P. *J. Pharmacol. Toxicol. Methods* **2010**, *62*, 1.
40. Folts, J. *Circulation* **1991**, *83*, 3.
41. van Giezen, J. J.; Berntsson, P.; Zachrisson, H.; Björkman, J. A. *Thromb. Res.* **2009**, *124*, 565.